

Cysteine-Cystine Photoregeneration for Oxygenic Photosynthesis of Acetic Acid from CO₂ by a Tandem Inorganic-Biological Hybrid System

Kelsey K. Sakimoto,^{†,‡} Stephanie J. Zhang,[†] Peidong Yang^{,†,‡,§}*

[†]Department of Chemistry, University of California-Berkeley, Berkeley, CA 94702. [‡]Materials Sciences Division, Lawrence Berkeley National Laboratory, Berkeley, CA 94702, USA.

Department of Materials Science and Engineering, University of California-Berkeley, Berkeley, CA 94702, USA. [§]Kavli Energy NanoSciences Institute, Berkeley, CA 94702.

KEYWORDS. Cadmium Sulfide, Titanium Dioxide, *Moorella thermoacetica*, Phthalocyanine, Solar-to-Chemical Production, Artificial Photosynthesis

ABSTRACT. Tandem “Z-scheme” approaches to solar-to-chemical production afford the ability to independently develop and optimize reductive photocatalysts for CO₂ reduction to multi-carbon compounds, and oxidative photocatalysts for O₂ evolution. To connect the two redox processes, molecular redox shuttles, reminiscent of biological electron transfer, offer an additional level of facile chemical tunability that eliminates the need for solid-state semiconductor junction engineering. In this work, we report a tandem inorganic-biological hybrid system capable of oxygenic photosynthesis of acetic acid from CO₂. The photoreductive catalyst consists of the bacterium *Moorella thermoacetica* self-photosensitized with CdS

nanoparticles at the expense of the thiol amino acid cysteine (Cys) oxidation to the disulfide form cystine (CySS). To regenerate the CySS/Cys redox shuttle, the photooxidative catalyst, TiO₂ loaded with co-catalyst Mn(II) phthalocyanine (MnPc), couples water oxidation to CySS reduction. The combined system *M. thermoacetica*-CdS+TiO₂-MnPc, demonstrates a potential biomimetic approach to complete oxygenic solar-to-chemical production.

Though they may project to outcompete natural photosynthesis, the conversion of solar energy into chemical bonds remains a daunting task for current artificial systems.¹ Many semiconductor light harvesters have been developed as both monolithic photoelectrodes and suspended nanoparticle photocatalysts.² However, the development of cheap, efficient and selective co-catalysts remains challenging for water oxidation and particularly for CO₂ reduction to multi-carbon compounds.³ Biomimetic co-catalysts that emulate the active sites of the proteins employed within natural photosynthesis have yet to fully capture the performance of their biological inspiration due to the inherent complexity of enzyme catalysis.⁴

To skirt these difficulties, several studies have recently demonstrated the use of whole cells and whole protein complexes in solar-to-chemical production schemes.⁵⁻⁸ We have recently shown the ability of the acetogenic bacterium *Moorella thermoacetica* to self-photosensitize by bio-precipitation of CdS nanoparticles, facilitating photosynthesis of acetic acid from CO₂.⁹ While this system demonstrates high efficiency photoreductive capabilities, the inorganic-biological hybrid organism operates at the expense of a sacrificial reductant, the thiol amino acid cysteine (Cys), which oxidizes to the disulfide form, cystine (CySS).

Direct photooxidation of water to O₂ by *M. thermoacetica*-CdS is infeasible due to the poor oxidative stability of many metal chalcogenides.¹⁰ We have thus taken a biomimetic

approach based on the tandem “Z-scheme” design, in which photoreduction and photooxidation are carried out by two separate light harvesters and co-catalysts.¹¹ To balance the CO₂ photoreduction of *M. thermoacetica*-CdS, TiO₂ nanoparticles were selected due to their well characterized performance as water oxidation photocatalysts as well as their high stability.¹²

Within tandem systems, two choices for linking photoreduction and photooxidation exist: 1) a direct solid-state junction and 2) a redox mediator. Though direct contact between the two semiconductor light absorbers could afford fast electrical conduction, optimization and engineering of the junction remains non-trivial due to the formation of detrimental charge transfer barriers.¹³ The junctions that form are highly dependent of the material, band structure, and doping of the semiconductor, rendering this approach non-general, thus requiring reoptimization with the discovery of new and better semiconductor light absorbers. Additionally, close proximity between oxidative and reductive processes may lead to significant back reactions at the opposing semiconductor resulting in net loss in photosynthetic products.¹⁴ In contrast, molecular redox mediators, which are widely employed within natural photosynthesis, afford a more facile connection to biological catalysts and offer a wide range of tunability via molecular synthetic chemistry as opposed to solid-state chemistry.

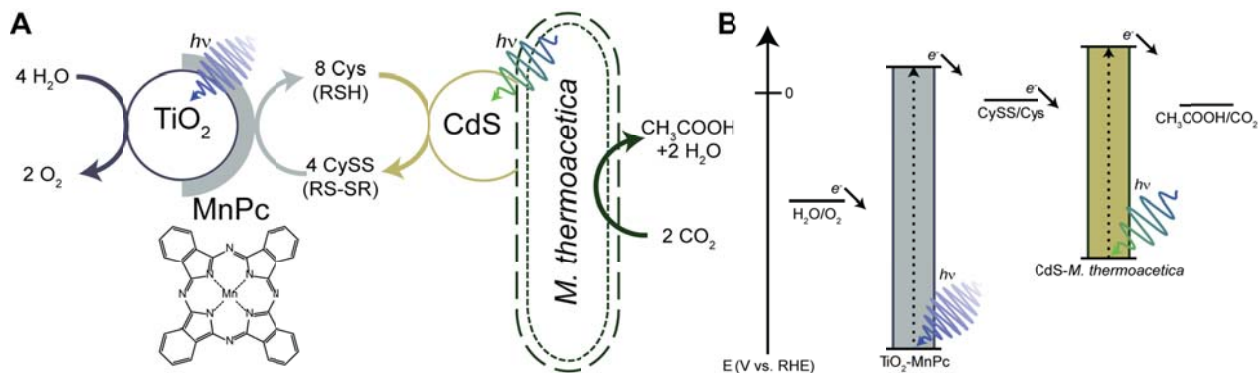


Figure 1. Schematic of the *M. thermoacetica*-CdS+TiO₂-MnPc Tandem System. A) Illumination of *M. thermoacetica*-CdS drives the reduction of CO₂ into acetic acid, coupled to the oxidation

of Cys to CySS. Co-illumination of TiO₂-MnPc drives the reduction of CySS back into Cys, coupled to oxidation of water to H₂O. B) Energy level diagram depicting the relative alignment of the TiO₂ and CdS with the relevant redox reactions.

Taking inspiration from biological redox processes, a biocompatible CySS/Cys redox couple (RSH/RSSR) was selected.¹⁵ As depicted in Fig. 1, the tandem system investigated here consists of a TiO₂ nanoparticle loaded with a manganese(II) phthalocyanine (MnPc) co-catalyst to reduce CySS back into Cys, rendering the formerly sacrificial reductant into a regenerative redox couple.

The choice of a selective CySS reduction co-catalyst was crucial to prevent degradation of the CySS/Cys redox couple. Bare TiO₂ alone has been shown to be a poor photocatalyst for CySS reduction due to irreversible oxidative degradation.^{16,17} Additionally, the inability of TiO₂ to absorb visible light severely limits its performance under solar illumination. Previous studies have reported on the electrochemical selectivity of various transition metal phthalocyanines (TMPc) to CySS reduction and Cys oxidation, and have suggested that MnPc displays the highest activity towards CySS reduction of the first row transition metals due to its stronger binding of Mn to CySS.¹⁸ Several first row TMPcs and unmetallated H₂Pc were tested under *in vitro* conditions suitable for *M. thermoacetica*-CdS photosynthesis by loading on to TiO₂ nanoparticles and measuring Cys production rate under illumination (5% sun, AM1.5G). Reflectance spectra of the TiO₂-TMPc photocatalysts were taken to confirm loading of MnPc (Fig. 2) and display strong retention of the absorption peaks of the molecular co-catalyst.

As presented in Tbl. 1, MnPc exhibited the highest activity for CySS reduction. The time series presented in Fig. 3 under an inert N₂ atmosphere as well 21% O₂ demonstrate that even in

the presence of an oxidant, photocatalyst illumination results in net Cys production and a steady state Cys concentration. However, the rate of CySS reduction eventually plateaus as the rate of oxidation back into CySS matches that of the forward reaction. However, this insight demonstrates that the TiO₂-MnPc photocatalyst system is compatible with aerobic conditions and net O₂ production.

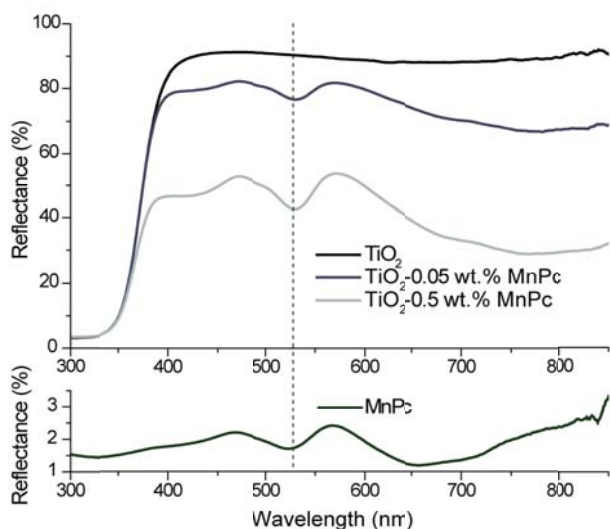


Figure 2. Reflectance Spectra of TiO₂-MnPc. Successful loading of increasing amounts of MnPc loaded onto TiO₂ as evidenced by sub-400 nm absorption. While the position of the peak at 530 nm remains consistent between the discrete and loaded MnPc, the lower energy peaks at ~650 nm broaden and redshift once loaded onto TiO₂.

Table 1. CySS Reduction Rate of Phthalocyanine Loaded TiO₂ Photocatalysts

Catalyst	Rate ($\mu\text{M Cys hr}^{-1}$)
No catalyst	53.0 \pm 9.3
MnPc (0.1 wt.%) ¹	65.9 \pm 4.6

MnPc (0.05 wt.%) ¹	130.1±8.4
MnPc (0.01 wt.%) ¹	75.9±3.3
FePc ²	61.9±4.5
CoPc ²	56.4±2.2
NiPc ²	87.7±18.7
CuPc ²	68.7±5.8
ZnPc ²	45.2±5.7
H ₂ Pc ²	75.5±12.8

¹Catalyst loading relative to mass of TiO₂. ²Equimolar to 0.05 wt.% MnPc. Standard deviation represents error associated with linear regression of kinetic data.

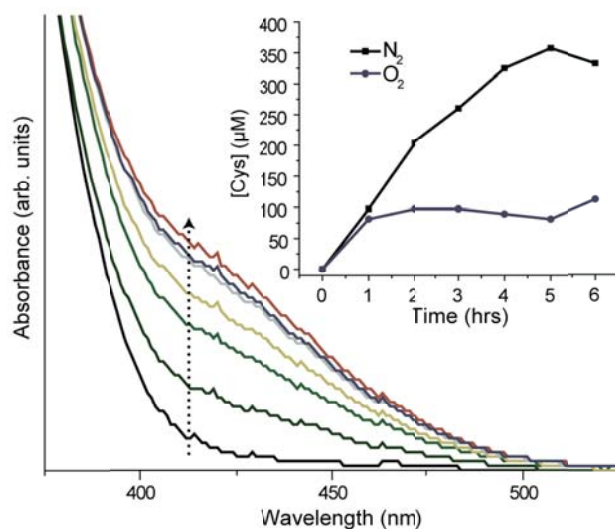


Figure 3. CySS Photoreduction Kinetics of TiO₂-MnPc. A colorimetric assay employing Ellman's reagent monitored the progress of Cys photogeneration. (*inset*) TiO₂-MnPc demonstrated net CySS photoreduction under both anaerobic and aerobic conditions.

The non-linear trend of CySS reduction activity with increasing an number of *d*-electrons deviates from the monotonic decreasing trend observed in previous reports.¹⁸ Specifically, we observe a local peak in activity for NiPc and CuPc which have exhibited the poorest dark

electrochemical activity. In addition, MnPc displays a significantly higher activity than all other tested Pc. While previous electrochemical studies employed relatively inert and non-interacting graphitic electrodes, reflectance spectra (Fig 2, S1) demonstrate a redshift in the low energy peaks around 650 nm, suggesting coupling between TiO₂ and MnPc. The solubility of TMPc in EtOH (the solvent used for loading) may play a role, as MnPc has the highest EtOH solubility, perhaps leading to more even loading on TiO₂ and a greater number of exposed active sites.¹⁹ However, both NiPc and CuPc have demonstrated lower solubility than FePc and CoPc, indicating that differences in coscatalyst loading fails to sufficiently explain the activity trend.

The spectrum of TiO₂-MnPc retains the distinct peak at 530 nm found in the neat MnPc spectrum (Fig. 2), whereas such spectral signatures are often lost in the other TiO₂-Pc photocatalysts suggesting either poor loading, or perhaps interactions between the TMPc and TiO₂ (Fig. S1). However, activity does not directly correlate with reflectance spectra, as NiPc and ZnPc which show the second highest and lowest activity, respectively, have similar reflectance spectra with deemphasized features.

Since previous studies were conducted as electrocatalysts in dark, the differences in activity observed here suggest TMPc visible light absorption has an effect on catalytic performance. TMPcs have been widely employed as visible and IR sensitizers of dye-sensitized solar cells (DSSCs) due to the favorable energy alignment of their HOMO and LUMO with the conduction band of TiO₂.²⁰ We do note that ZnPc, a common visible light sensitizer in DSSCs, demonstrates the lowest activity, perhaps due to the favorable charge injection from ZnPc to TiO₂ that would impede CySS reduction.

The activity of NiPc deviates most drastically from previous reports. While Zagal, et al. report NiPc as one of the least catalytically active for CySS reduction, photocatalytically, NiPc

was the second most active behind MnPc. Analysis of the MO diagram of NiPc shows that the HOMO-LUMO charge transfer is a ligand-to-metal charge transfer (LMCT) from the Pc a_{1u} to the Ni $3d_{x^2-y^2}$ centered b_{1g} .²¹ This shift of electron density towards the metal active site under illumination may improve CySS binding and increase reduction activity. In contrast, FePc and CoPc, the least photocatalytically active, exhibit largely metal-to-ligand charge transfer (MLCT) which may disfavor CySS binding. A similar LMCT argument may explain the higher activity of CuPc. H₂Pc also demonstrates reasonable activity towards CySS reduction despite not having a metal site to facilitate disulfide binding. However, the close proximity of two hydrogens may favor a proton-coupled electron transfer.

Illumination of various combinations of *M. thermoacetica*-CdS and TiO₂-MnPc demonstrated that the CySS photoregenerative catalyst effectively pairs with the CO₂ photoreductive catalyst (Fig 4). When only *M. thermoacetica*-CdS was illuminated, the rate of acetic acid production leveled off after roughly 1 day, below the stoichiometric limit set by Cys as limiting reagent (i.e. no photoregeneration). Similarly, combination of TiO₂-MnPc with CdS-free *M. thermoacetica* cells yielded negligible acetate production (Fig. 4A). While the band gap of TiO₂ is thermodynamically sufficient to drive microbially catalyzed CO₂ reduction, the process remains kinetically unfavorable due to the poor interface between TiO₂-MnPc and *M. thermoacetica*. TiO₂ may also photosterilize *M. thermoacetica* in the absence of CdS nanoparticles via the formation of reactive oxygen species (ROS).²² Finally, the combination of *M. thermoacetica*-CdS for CO₂ reduction to acetic acid and Cys oxidation, coupled with TiO₂-MnPc for CySS reduction and water oxidation produced a net amount of acetic acid at a higher rate than *M. thermoacetica*-CdS alone, and above the stoichiometric limit of Cys, clear evidence of CySS/Cys as a regenerative redox couple. The photoprotective role of TiO₂ (in addition to the

protection afforded by CdS alone) may also help to explain the higher photosynthetic rate of *M. thermoacetica*+TiO₂-MnPc compared to *M. thermoacetica*-CdS alone.²³ Comparison of electron yields for the reduced product (acetic acid) and oxidative products (O₂ and CySS) show comparable stoichiometries (Fig. 4B). A slight excess of oxidative products are indicated due to potential loss of acetic acid towards *M. thermoacetica* biomass.²⁴ Additionally, as CySS participates within the redox cycle, CySS derived electron equivalents indicated in Fig. 4B are slightly overestimated.

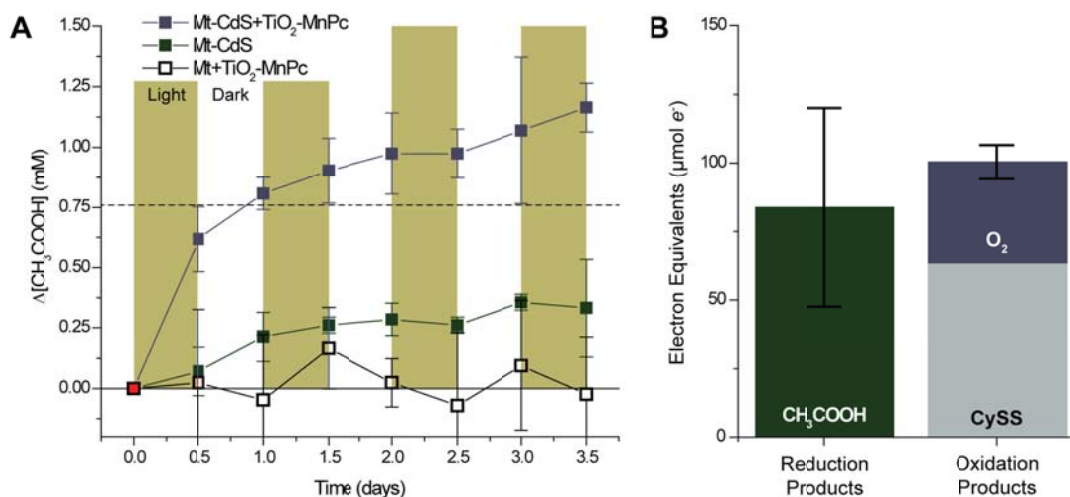


Figure 4. Photosynthetic Performance of *M. thermoacetica*-CdS and TiO₂-MnPc Tandem System. A) Comparison of *M. thermoacetica*-CdS and TiO₂-MnPc with controls show greater acetic acid production from the combination of the tandem system. Both *M. thermoacetica*-CdS only and *M. thermoacetica*+TiO₂-MnPc controls showed lower acetic acid production below the stoichiometric limit imposed by Cys (dashed line). B) Comparison of acetic acid (8e⁻) and O₂ (4e⁻) yields after 3.5 days. Electrons potentially derived from the next oxidation of Cys to CySS (2e⁻) indicated to balance electron equivalents between acetic acid and O₂. All values represent the average and standard deviation of triplicate experiments.

While the current system demonstrates reasonable net kinetic performance, several improvements could be made to further increase the photosynthetic rate. As seen in both Fig. 3 (inset) and Fig. 4A, the rate of CySS reduction or acetic acid production begins to decrease from the initial rate, likely due to the effects of O₂ accumulation. As the partial pressure of O₂ rises, the back reaction of Cys oxidation begins to compete, giving a steady state concentration of Cys below the ~6 mM desired for high CO₂ reduction rates by *M. thermoacetica*-CdS. Additionally, the O₂ sensitivity of CdS and the anaerobic *M. thermoacetica* likely limit their performance at higher O₂ concentrations.²⁵ While engineering approaches such as gas purging could limit the detrimental effects of O₂, a more elegant solution would call for physically separating the two incompatible processes through either physical space, or via a selective membrane.²⁶ While physically separating the oxidative and reductive photocatalysts would create significant difficulties for solid-junction nanoparticle tandem systems, the use of a molecular redox shuttle enabled by diffusional or convective transport renders this design readily accessible.

The limited light absorption of TiO₂ and CdS likely bottlenecks the solar-to-chemical efficiency of the current system. Exploration of the semiconductor parameters space may yield lower bandgap semiconductors to raise the theoretical limit on solar-conversion efficiency. Due to the relative ease of engineering molecular rather than solid-state interfaces, the various components of this modular tandem inorganic-biological hybrid system may be switched out as newer, better performing materials become available. With these advances, this paradigm holds promise for the future of advanced solar-to-chemical production.

ASSOCIATED CONTENT

Supporting Information.

Figure S1-2

Materials and Methods.

This material is available free of charge via the Internet at <http://pubs.acs.org>.

AUTHOR INFORMATION

Corresponding Author

*p_yang@berkeley.edu

Author Contributions

The manuscript was written through contributions of all authors. All authors have given approval to the final version of the manuscript.

Notes

The authors declare no competing financial interests.

ACKNOWLEDGMENT

K.K.S.acknowledges support from the NSF Graduate Research Fellowship Program under grant DGE-1106400. Solar-to-chemical production experiments were supported by the NSF under grant DMR-1507914. The authors thank J.J. Gallagher and M.C.Y. Chang for the original inoculum of *M. thermoacetica* ATCC 39073.

REFERENCES

- (1) Kim, D.; Sakimoto, K. K.; Hong, D.; Yang, P. *Angew. Chemie Int. Ed.* **2015**, *54* (11), 3259–3266.
- (2) Osterloh, F. E. *Chem. Soc. Rev.* **2013**, *42* (6), 2294–2320.
- (3) Kumar, B.; Llorente, M.; Froehlich, J.; Dang, T.; Sathrum, A.; Kubiak, C. P. *Annu. Rev. Phys. Chem.* **2012**, *63*, 541–569.
- (4) Magnuson, A.; Anderlund, M.; Johansson, O.; Lindblad, P.; Lomoth, R.; Polivka, T.; Ott, S.; Stensjö, K.; Styring, S.; Sundström, V.; Hammarström, L. *Acc. Chem. Res.* **2009**, *42* (12), 1899–1909.
- (5) Torella, J. P.; Gagliardi, C. J.; Chen, J. S.; Bediako, D. K.; Colón, B.; Way, J. C.; Silver, P. A.; Nocera, D. G. *Proc. Natl. Acad. Sci.* **2015**, *112* (8), 2337–2342.
- (6) Liu, C.; Gallagher, J. J.; Sakimoto, K. K.; Nichols, E. M.; Chang, C. J.; Chang, M. C. Y.; Christopher, J.; Yang, P.; *Nano Lett.* **2015**, *15* (5), 3634–3639.
- (7) Nichols, E. M.; Gallagher, J. J.; Liu, C.; Su, Y.; Resasco, J.; Yu, Y.; Sun, Y.; Yang, P.; Chang, M. C. Y.; Chang, C. J. *Proc. Natl. Acad. Sci.* **2015**, *112* (37), 11461–11466.
- (8) Wang, W.; Chen, J.; Li, C.; Tian, W. *Nat. Commun.* **2014**, *5*, 4647.
- (9) Sakimoto, K. K.; Wong, A. B.; Yang, P. *Science* (80-.). **2016**, *351* (6268), 1–17.
- (10) Meissner, D.; Memming, R. *J. Phys. Chem.* **1988**, *92*, 3476–3483.
- (11) Kudo, A.; Miseki, Y. *Chem. Soc. Rev.* **2009**, *38* (1), 253–278.

- (12) Chen, X.; Mao, S. S. *Chem. Rev.* **2007**, *107* (7), 2891–2959.
- (13) Resasco, J.; Zhang, H.; Kornienko, N.; Becknell, N.; Lee, H.; Guo, J.; Briseno, A. L.; Yang, P. *ACS Cent. Sci.* **2016**, acscentsci.5b00402.
- (14) Liu, C.; Tang, J.; Chen, H. M.; Liu, B.; Yang, P. *Nano Lett.* **2013**, *13* (6), 2989–2992.
- (15) Paulsen, C. E.; Carroll, K. S. *Chem. Rev.* **2013**, *113* (7), 4633–4679.
- (16) Nosaka, A. Y.; Tanaka, G.; Nosaka, Y. *J. Phys. Chem. B* **2012**, *116*, 11098–11102.
- (17) Machado, A. E. H.; França, M. D.; Velani, V.; Magnino, G. A.; Velani, H. M. M.; Freitas, F. S.; Müller, P. S.; Sattler, C.; Schmücker, M. *Int. J. Photoenergy* **2008**, 2008.
- (18) Zagal, J. H.; Herrera, P. *Electrochim. Acta* **1985**, *30* (4), 449–454.
- (19) Ghani, F.; Kristen, J.; Riegler, H. *J. Chem. Eng. Data* **2012**, *57*, 439–449.
- (20) Giribabu, L.; Vijay Kumar, C.; Gopal Reddy, V.; Yella Reddy, P.; Srinivasa Rao, C.; Jang, S. R.; Yum, J. H.; Nazeeruddin, M. K.; Grätzel, M. *Sol. Energy Mater. Sol. Cells* **2007**, *91* (17), 1611–1617.
- (21) Liao, M. S.; Scheiner, S. *J. Chem. Phys.* **2001**, *114* (22), 9780–9791.
- (22) Ireland JC, Klostermann P, Rice EW, C. R. *Appl. Environ. Microbiol.* **1993**, *59* (5), 1668–1670.
- (23) Holmes, J. D.; Smith, P. R.; Evans-Gowing, R.; Richardson, D. J.; Russel, D. A.; Sodeau, J. R. *Photochem. Photobiol.* **1995**, *62* (6), 1022–1026.
- (24) Daniel, S. L.; Hsu, T.; Dean, S. I.; Drake, H. L. *J. Bacteriol.* **1990**, *172* (8), 4464–4471.

(25) Karnholz, A.; Küsel, K.; Gößner, A.; Drake, H. L.; Schramm, A. *Appl. Environ. Microbiol.* **2002**, 68 (2), 1005.

(26) Giddings, C. G. S.; Nevin, K. P.; Woodward, T.; Lovley, D. R.; Butler, C. S. *Front. Microbiol.* **2015**, 6 (MAY), 1–6.

TOC Graphic

